www.elsevier.com/locate/jssc

Toward a better understanding of the magnetocaloric effect: An experimental and theoretical study of $MnFe_4Si_3$

Olivier Gourdon, Michael Gottschlich, Joerg Persson, Clarina de la Cruz, Vaclav Petricek, Michael A McGuire, Thomas Brückel

PII: S0022-4596(14)00193-5
DOI: http://dx.doi.org/10.1016/j.jssc.2014.05.001
Reference: YJSSC18465

To appear in: *Journal of Solid State Chemistry*

Received date: 13 February 2014
Revised date: 29 April 2014
Accepted date: 5 May 2014

Cite this article as: Olivier Gourdon, Michael Gottschlich, Joerg Persson, Clarina de la Cruz, Vaclav Petricek, Michael A McGuire, Thomas Brückel, Toward a better understanding of the magnetocaloric effect: An experimental and theoretical study of $MnFe_4Si_3$, *Journal of Solid State Chemistry*, http://dx.doi.org/10.1016/j.jssc.2014.05.001

Toward a better understanding of the magnetocaloric effect: An experimental and theoretical study of $MnFe_4Si_3$

Olivier Gourdon, *[a] Michael Gottschlich,[b] Joerg Persson,[b] Clarina de la Cruz,[c] Vaclav Petricek,[d] Michael A McGuire [e] and Thomas Brückel [f]

[a] *Los Alamos Neutron Scaterring Center, National Laboratory, Los Alamos, NM, 87545, USA*

[b] *Jülich Center for Neutron Science JCNS-2 and Peter Grünberg Institut PGI-4, JARA-FIT, Forschungszentrum Jülich 52425 Jülich, Germany.*

[c] *Quantum Condensed Matter Division, Spallation Neutron Source, Oak Ridge National Laboratory, Oak Ridge, Tennessee 37831, USA*

[d] *Institute of Physics ASCR v.v.i., Na Slovance 2, 182 21 Praha, Czech Republic.*

[e] *Materials Science and Technology Division, Oak Ridge National Laboratory, Oak Ridge, Tennessee 37831, USA*

[*] *Corresponding Author E-mail: gourdono@lanl.gov*

Abstract

The intermetallic compound $MnFe_4Si_3$ has been studied by high-resolution Time of Flight (TOF) neutron powder diffraction. $MnFe_4Si_3$ crystallizes in the hexagonal space group $P6_3/mcm$ with lattice constants of a=b=6.8043(4) Å and c=4.7254(2) Å at 310 K. Magnetic susceptibility measurements show clearly the magnetic transition from paramagnetism to ferromagnetism at about 302(2) K. Magnetic structure refinements based on neutron powder diffraction data with and without external magnetic field reveal strong evidence on the origin of the large magnetocaloric effect (MCE) in this material as a partial reordering of the spins between ~270 K and 300 K. In addition, electronic structure calculations using the self-consistent, spin-polarized Tight Binding-Linear MuffinTin Orbital (TB-LMTO) method were

Journal Name

Dynamic Article Links#►

Cite this: DOI: 10.1039/c0xx00000x

www.rsc.org/xxxxxx

ARTICLE TYPE

also accomplished to address the “coloring problem” (Mn/Fe site preference) as well as the unique ferromagnetic behaviour of this intermetallic compound.

Introduction

In the past decade, a rapid development of a new magnetic refrigeration technology, based upon the magnetocaloric effect (MCE), has attracted an immense increase in interest in magnetic materials. Magnetic refrigeration, which is based on the entropy changes of magnetic materials in an applied magnetic field, exhibits more considerable advantages than conventional vapour-cycle refrigeration, such as high energy efficiency, small volume, ecological cleanliness, etc. Until recently, the best candidate known were gadolinium (Gd) based materials such as $Gd_5Ge_2Si_2$ [1-5] or arsenides such as $MnFeP_{1-x}As_x$. [6-9] However, the high cost of Gd and the toxicity of As make it questionable whether current materials based on either technology could be deployed commercially. Therefore, materials research in the magnetic cooling field has been mainly focused on the search for new low cost/environment friendly materials displaying satisfactory MCEs.

As part of an effort to gain a better understanding of the chemical and physical parameters which drive the MCE and to potentially design new magnetic materials, we reinvestigated the magnetic and the crystallographic structure of $MnFe_4Si_3$. Our interest of studying that specific Mn/Fe composition was driven by a recent work reported by Songlin et al.[10] showing a unique MCE effect for that specific Mn/Fe composition along the $Mn_{1-x}Fe_xSi_3$ series. They reported the magnetic susceptibility of $MnFe_4Si_3$ shows clearly that this phase undergoes a sharp paramagnetic-ferromagnetic transition at 302(2) K associated with a MCE of up to 3 J/ kg K^{-1}, by applying an external magnetic field of only 3 Tesla (see Figure 1). Our studies were performed at various temperature and magnetic field in order to understand the response of such external contributions to the magnetic and the crystallographic structures. Our magnetic structure refinements based on neutron powder diffraction data under magnetic field near room temperature strongly suggest that the origin of the MCE properties in this class of material is a partial reordering of the spins. Furthermore, electronic structure calculations using the self-consistent, spin-polarized TB-LMTO method were also performed to understand the unique physical properties of the $MnFe_4Si_3$ intermetallic compound, especially the "colouring problem" (Mn/Fe site preference), the low temperature ferromagnetism, but also its almost half-metallic behaviour.

Experimental Section

$MnFe_4Si_3$ polycrystalline samples have been prepared by melting with induced current method under Argon. For further information on the preparation technique please see reference [11] and references within. Every batch was melted and annealed at least four times to ensure homogeneity. Mn (Aldrich, 99.99%), Fe (Aldrich, 99.99%) and Si (Aldrich, 99.99%) were used as starting materials. The Mn metal pieces were preliminary melted under argon so that oxidation could be easily removed from the surface. All final products remain with a metallic lustre and are visibly stable upon exposure to both air and moisture over several weeks.

The phase purities of the products were analysed using energy dispersive spectroscopy (EDS) by a JEOL 840A scanning electron microscope, equipped with an IXRF system Iridium X-ray analyser with a Kevex Quantum thin-window Si(Li) detector for quantitative chemical analysis with Si as the internal standard. Data have been collected on various different points giving a homogeneous composition of the samples of $Mn_{0.97(3)}Fe_{4.1(2)}Si_3$ consistent with the composition expected. No significant oxygen contamination was observed during the data collection.

The dc magnetization as a function of temperature from 1.8 to 320 K and the magnetic field (from 0 to 4 Tesla) was measured on a Quantum design (QD) Magnetic Property Measurement System (MPMS). Temperature-dependent magnetization data were collected after the $MnFe_4Si_3$ polycrystalline sample was placed in a gel-capsule fixed in a straw by measuring the field-cooled (FC) magnetization.

Due to the nearly indistinguishable X-ray scattering factor between Mn and Fe (one electron apart), neutron powder diffraction experiments were performed on a ca. 4 g powder sample of $MnFe_4Si_3$ to achieve better resolution of the transition metal site occupancies. Indeed, the elastic neutron cross section for Mn (1.75 barn) and Fe (11.22 barn) are significantly different, which allows us to refine site distributions accurately. Moreover, as magnetic behaviour is expected for $MnFe_4Si_3$, neutron scattering could give unique information on the magnetic ordering. Therefore, TOF neutron powder diffraction data were collected at the Spallation Neutron Source (SNS), Oak Ridge National Laboratory on the new powder diffractometer POWGEN. Differing from nearly all other time-of-flight (TOF) neutron powder diffractometers, the design of POWGEN is based on combining the diffracted neutrons collected at all angles into a single profile rather than assigning them to series of different profiles that traditionally were based on grouping detectors according to scattering angle. Such a unique approach yields to a high count rate while preserving good resolution $\Delta d/d$ = 0.0015 at a d = 1 Å. Further information on the design of

POWGEN could be found in reference [12] and references therein. Data were collected at 310 K, 300 K, 270 K, 250 K, 220 K, 190 K, 160 K, 130 K, 100 K, 80 K, 50 K, 30 K and 10 K in that specific order. For each temperature data collections have been performed using a unique center wavelength (CWLs) of 1.066 Å, which covers a d-spacing range from 0.29 Å to 3.30 Å. This energy bandwidth has been ideally chosen in order to have accurate information on the nuclear/magnetic structure as well as on the atomic displacement parameters (ADPs).

Additional neutron powder diffraction data were also collected under 0 T and 3 T magnetic field on the same sample in the vicinity of room temperature on the high-resolution neutron powder diffractometer HB2A at the High Flux Isotope Reactor at Oak Ridge National Laboratory, using 12'-31'-6' collimation and a wavelength of 2.41 Å {Ge (113)}. Based on the expected ferromagnetic behaviour of the materials and to avoid a strong preferred orientation of the grain under magnetic field, the loose powder was pelletized and the pellets were adjusted into the vanadium can. More details about the HB2A instrument can be found in Reference 13.

The crystallographic structures were refined using JANA2006 software [14] using the $MnFe_4Si_3$ structure, known from the literature, [15] as a starting model. All the refinements were performed to obtain accurately unit cell parameters, atomic positions, and ADPs. Background coefficient, scale factors, isotropic strain terms in the profile function and absorption were also refined for a total of 27 parameters (16 profiles + 11 atomic parameters) using the centrosymmetric space group $P6_3/mcm$ for the paramagnetic phase. At lower temperature no additional magnetic reflections are detected, but an intensity increase of some reflections is observable and consistent with the ferromagnetism. Magnetic refinements were also performed using JANA2006 .[14] The magnetic scattering formalism has been recently implemented into the program which used a unique concept of superspace groups to treat magnetic groups. [16, 17] Using such description the ferromagnetic ordering observed in $MnFe_4Si_3$ is associated to a magnetic modulation vector of **k**=0. Since this treatment is similar to the use of classical Shubnikov magnetic space group this last approach will be presented thereafter. Among all the possible magnetic space groups *$P6_3/mc'm'$* has been considered since it was giving the more reliable refinements. A full description of the temperature-dependence of magnetic structures refinements will be given in the following section entitled "Experimental results".

Theoretical electronic structures of various model structures of $MnFe_4Si_3$ were calculated self-consistently by using the tight-binding, linear muffin-tin-orbital (TB-LMTO) method [18-21] within

the atomic sphere approximation (ASA) using the Stuttgart code.[22] Exchange and correlation were treated in a local spin density approximation (LSDA).[23] All relativistic effects except spin-orbit coupling were taken into account using a scalar relativistic approximation.[24] Within the ASA, space is filled by overlapping Wigner-Seitz (WS) atomic spheres. The radii of these WS spheres were obtained by requiring the overlapping potential to be the best possible approximation to the full potential according to an automatic procedure. [25] The WS radii for the atomic sites determined by this procedure are in the ranges 1.4-1.535 Å for Mn and Fe sites and 1.455-1.481 Å for Si sites. The basis set included 4s and 4p orbitals for Si and 4s, 4p, and 3d orbitals for Mn and for Fe. The reciprocal space integrations to determine the self-consistent total energies and charge densities, densities of states (DOS) curves, and crystal orbital Hamilton population (COHP) [26] curves were performed using the tetrahedron method [27] using 96 **k**-points, all-model structures in the irreducible wedges of the corresponding Brillouin zones.

Experimental Results

A. Magnetic behaviour of $MnFe_4Si_3$

Temperature dependence of the *dc* magnetic susceptibility is shown in Figure 1(a). It shows clearly strong evidence of a paramagnetic to ferromagnetic transition at about 302 (2) K. Above that temperature, the reciprocal magnetic susceptibility, not shown, obeys to the Curie-Weiss law with an average value of the effective magnetic moment equal to 1.7(1) μ_B per transition metal atom. Figure 1(b) illustrates the magnetic field dependence of the isothermal magnetic measurements (M(*H*)) in the 270 K to 320 K temperature range (5K steps). These measurements have been performed to evaluate the MCE in the $MnFe_4Si_3$ compound. Indeed, by measuring the isothermal magnetization around T_c as a function of the magnetic field, it is possible to have access to the magnetic entropy change (ΔS_m) by means of the equation:

$$\Delta S_m = \int_{H_1}^{H_2} \left(\frac{\partial M}{\partial T} \right)_H dH \qquad (1)$$

This equation (1) can be integrated numerically in the desired range of temperatures and magnetic fields on the basis of the set of experimental magnetization isotherms I(*H*) at different

temperatures T_1, T_2, ….The derivative δM/δT can also be calculated numerically :

$$|\Delta S_m| = \sum_i \frac{1}{T_{i+1} - T_i}(M_i - M_{i+1})\Delta H_i, \qquad (2)$$

Such numerical calculations of ΔS_m in MCE materials based on magnetization isotherms were previously performed by McMichael et al.,[28] Dan'kov et al.,[29] Pecharsky and Gschneider [30] and other authors.

In figure 1c is shown the entropy change around T_c between 0T and 3T calculated based on the isothermal magnetization measurements (Figure 1b) using eq. (2). Maximum entropy of ΔS_{Mag} ~ 3 J/Kg. K is observed ~ 300 K and most (half of the entropy change level) of the MCE process arises between 280 and 320 K. This value is in good agreement with the one measured by Songlin et al. (maximum entropy changes of 4 J/Kg.K for a magnetic field variation of 5 T).[10]

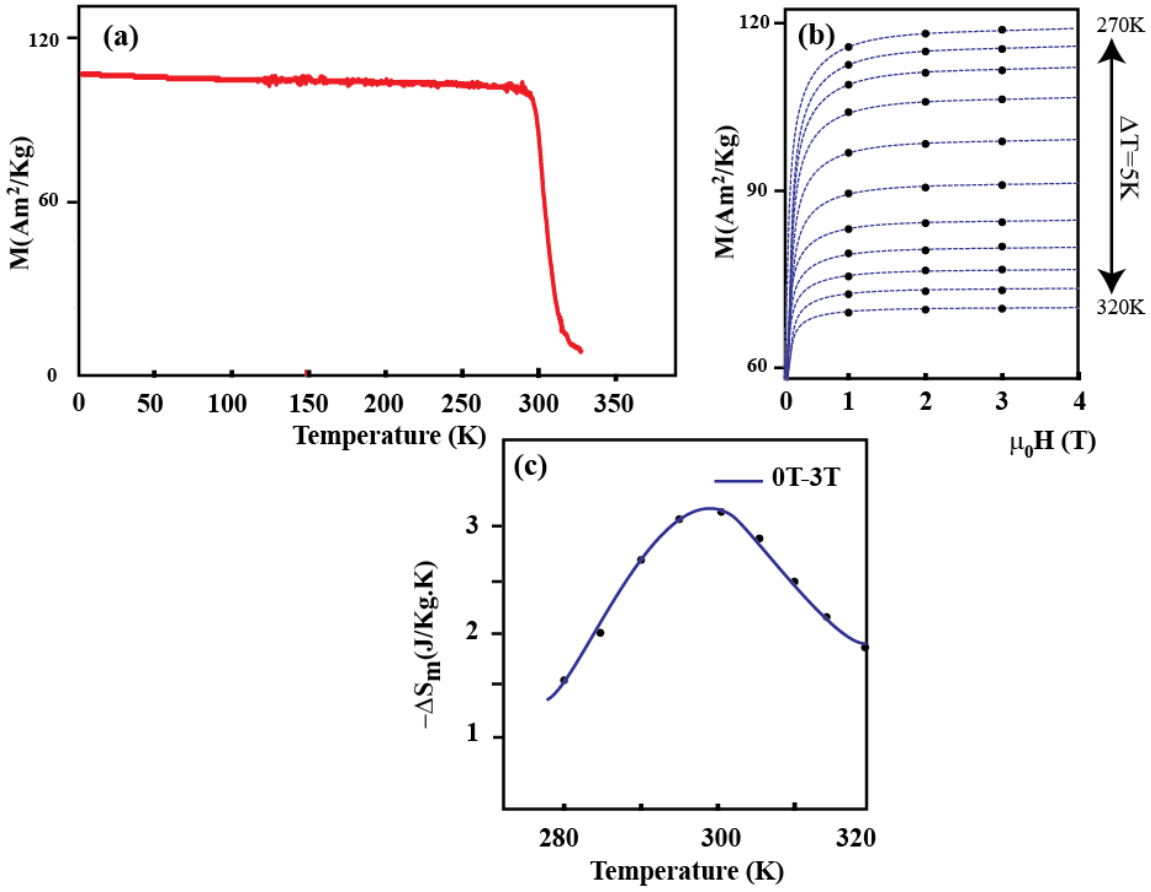

Figure 1. Temperature dependence of the (a) dc magnetization, (b) field dependence of the magnetization at various temperatures from 270 K to 320 K (black dots) and (c) entropy change, between 0 T and 3 T, calculated based on the magnetization measurements using the eq. (2). Blue lines in figures (b) and (c) are guides for the eyes. See text for further details.

B. Nuclear/Magnetic structure determination of $MnFe_4Si_3$

To gain a better understanding of the structural/magnetic arrangement in $MnFe_4Si_3$, temperature-dependent neutron diffraction measurements on a polycrystalline sample were conducted. At 310 K, $MnFe_4Si_3$ is paramagnetic and exhibits a hexagonal structure with space group $P6_3/mcm$ and lattice constants of a=b=6.8043(4) Å and c=4.7254(2) Å. Refinements have been performed using the structural model previously reported in the literature .[15] Figure 2 shows the observed and calculated neutron diffraction patterns collected on POWGEN at 310K. Refinement of the neutron data, which included background coefficients, scale factors, profile functions, and absorption coefficients, atomic position parameters and atomic displacement parameters,

smoothly converged to a reasonable solution with a goodness of fit (gof) value of 1.83 for R= 4.12% for 27 parameters. To elucidate the arrangement and concentration of Mn and Fe, the occupancies of the two metallic sites (M1 and M2) were also refined. The refined chemical composition of $Mn_{0.99(2)}Fe_{4.01(2)}Si_3$ is in exceptionally good agreement with the loaded composition ($MnFe_4Si_3$). Table 1 summarizes the refined atomic parameters and the equivalent ADPs for $Mn_{0.99(2)}Fe_{4.01(2)}Si_3$ at 310 K.

Table 1. Atomic Parameters and Equivalent Displacement Parameters ($Å^2$) for $Mn_{0.99(2)}Fe_{4.01(2)}Si_3$ at 310 K.

Atom	Occ. Mn/Fe	x	y	z	U_{eq}
M1	0.016(4)/0.984	1/3	2/3	0	0.00343(11)
M2	0.320(4)/0.680	0.24269(4)	0.24269(4)	-1/4	0.00506(11)
Si	-	0	0.3995(1)	-1/4	0.0045(2)

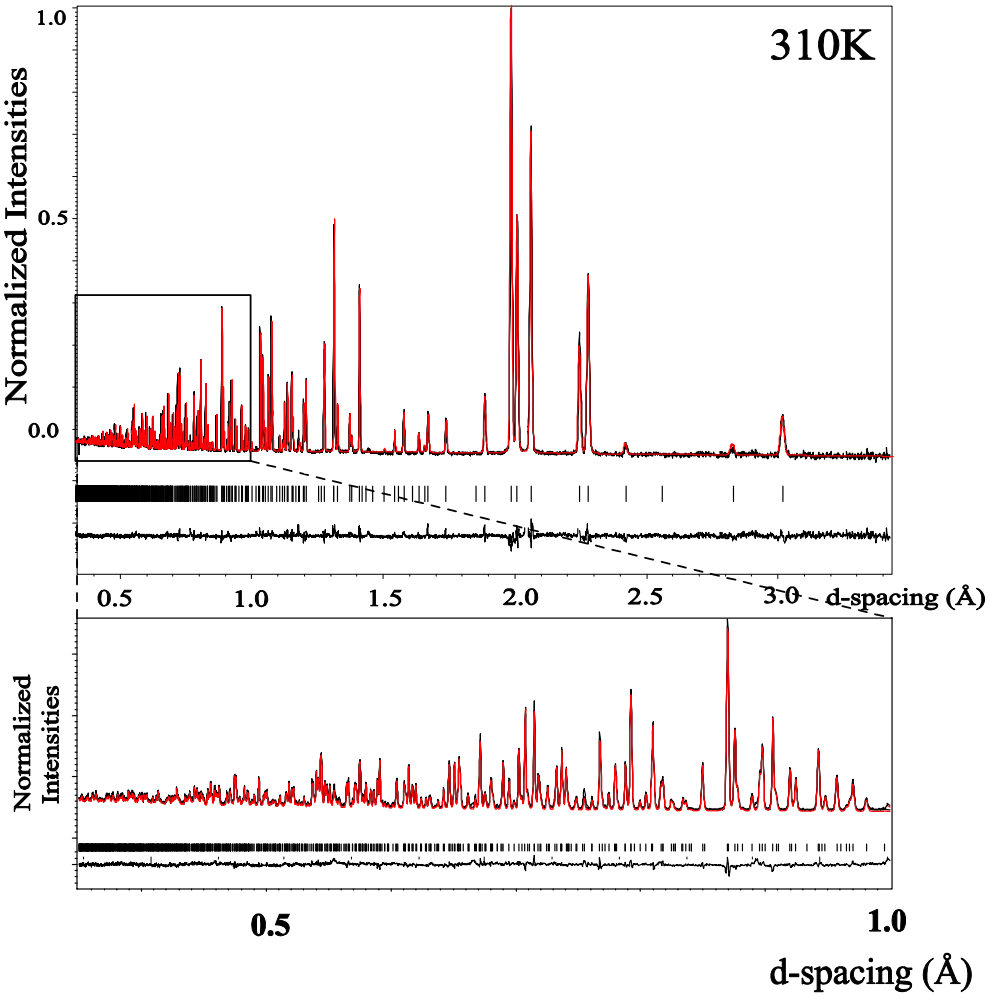

Figure 2. $Mn_{0.99(2)}Fe_{4.01(2)}Si_3$ neutron powder pattern obtained on POWGEN at 310 K. Red and black lines indicate normalized profile and calculated profile, respectively. Tick marks below profile indicate the positions of all allowed reflections, and the difference curve is shown below the tick marks on the same scale (d-spacing range 0.30 – 3.4 Å). The inset presents an expanded region of the d-spacing range between 0.30 and 1.00 Å.

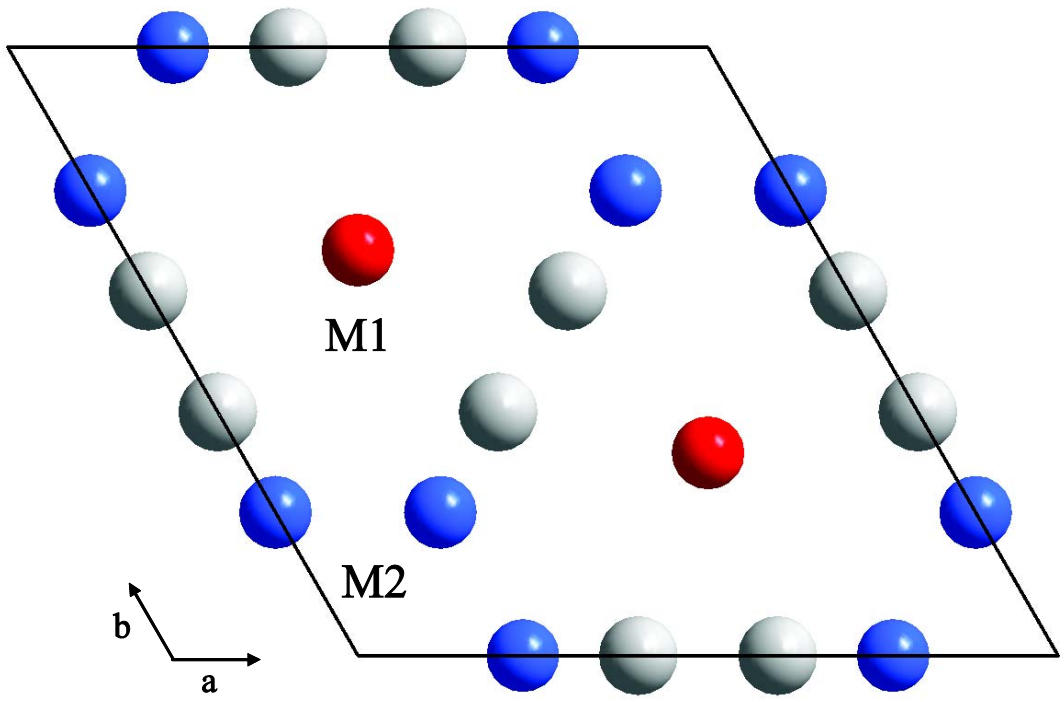

Figure 3. View along the *c*-axis of the $MnFe_4Si_3$ unit cell. Red, blue and grey spheres represent M1, M2 and Si atomic sites, respectively. M1 and M2 refer to the two specific mixed Mn/Fe sites (see text for details).

Figure 3 illustrates a view of the $MnFe_4Si_3$ hexagonal unit cell along the *c* axis. One classical way to explain this structure is to describe the local environments formed by the two metal sites (M1 and M2) which occupy the Wyckoff positions *4g* and *6d*, respectively (Figure 4). The M1 site which is, at 310 K, surrounded by 6 equidistant Si atoms at 2.3894 (5) Å, occupy a distorted octahedral site. This $[M1Si_6]$ polyhedron is bicapped, through Si_3 triangular faces, by two additional M1 atoms. This results in $[M1Si_6]$ polyhedra sharing triangular faces with their analogues to form quasi infinite $^1_\infty[M1Si_3]$ chains along the c-axis. The M1-M1 distances are the shortest distances observed in the crystal structure and are directly associated with the *c* parameter: $d_{M1\text{-}M1}=c/2=2.3628$ (2) Å. Surrounding these chains M2 atoms are connected forming vacant $[\square(M2)_6]$ distorted octahedron with M2-M2 distances of 2.9054(3) Å. These $[\square(M2)_6]$ octahedra share triangular faces to form quasi infinite $^1_\infty[\square(M2)_3]$ chains, also along the c-axis.

The metal-site preference (Mn and/or Fe) into the sites M1 and M2, also called "the coloring

problem" is directly associated with the existence of these two different local environments. Various similar intermetallic compounds such as, for example, $Gd_{5-x}\mathbf{M_xTt_4}$ (**M** = Zr, Hf; **Tt** = Si, Ge) [31] present such structural complexity which have been explained using both geometric and electronic considerations. The last section entitled "Electronic Structure calculations" will address some of the energetic factors which control the site preferences into $MnFe_4Si_3$: "site energies" and "bond energies".

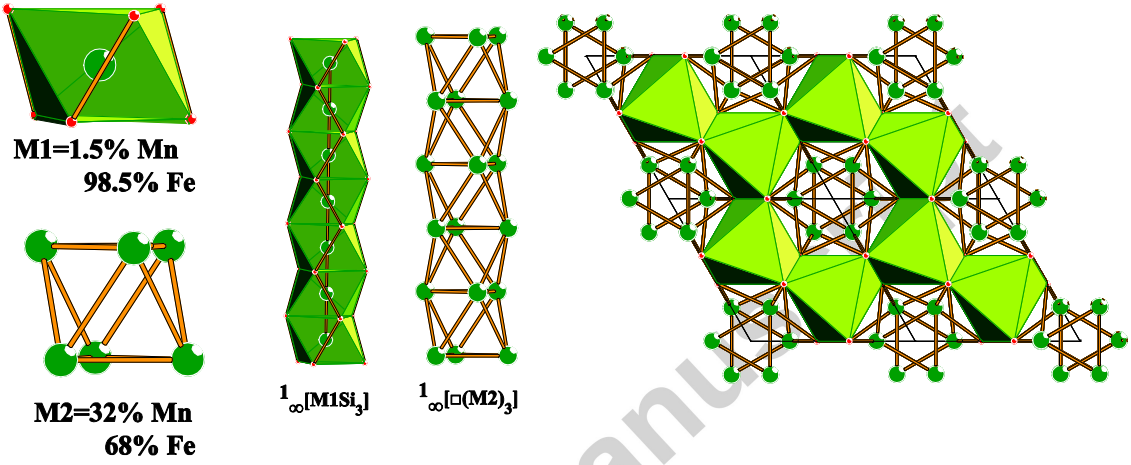

Figure 4. Representation of the different connections between the polyhedra formed by the M1 and M2 atoms.

Below 300 K and as illustrated in Figure 5 an increase of the intensity of some specific diffraction peaks is in good agreement with the magnetic measurements which indicate a ferromagnetic ordering of the spins at lower temperatures. Therefore, various magnetic models have been attempted and the magnetic space group P*6$_3$/mc'm'* has been considered in the final refinements as the most suitable. Using that magnetic space group, neutron data collected at 300 K, 270 K, 250 K, 220 K, 190 K, 160 K, 130 K, 100 K, 80 K, 50 K, 30 K and 10 K have been refined. Figures 6 and 7 illustrate the major features observed based on the magnetic refinements. In figure 6(a) the evolution of the cell parameters shows an atypical behaviour for the (*a,b*) cell parameters. Whereas the *c* cell parameter increases classically as the temperature increases, the (*a,b*) cell parameters decrease between 10 K and 100 K but also above the Curie temperature 300 K. Figures 6(b) and 6(c) also illustrate that above the magnetic transition the ADPs values decrease. Such correlations could potentially suggest strong magnetoelastic coupling in this class of materials which are still under investigation.[29] The magnetoelastic coupling act between the

magnetic moments and the lattice modifying the spin waves in two different ways. The static deformations of the crystal, induced the ordered moments introducing new anisotropic terms in the spin-wave Hamiltonian and the dynamic time-dependent modulations of the magnetic moments furthermore interfere with the lattice vibrations. To discuss such effects associated with magnon-phonon interactions further inelastic scattering experiments in the meV energy range should be performed.

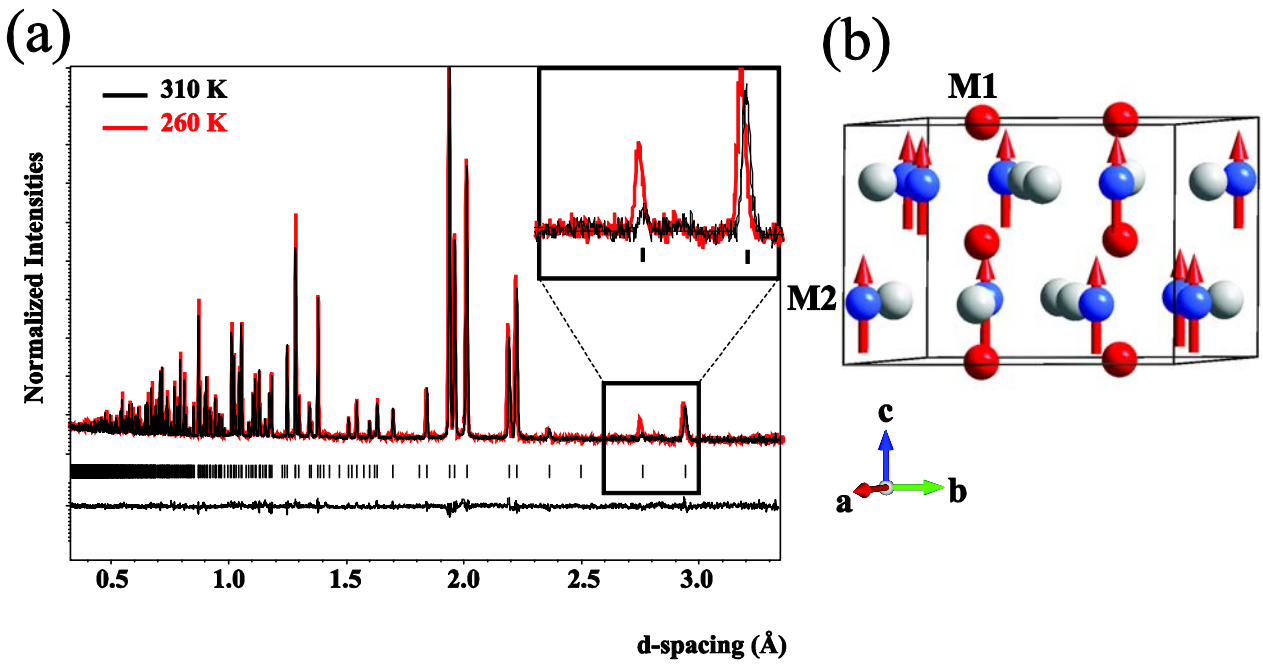

Figure 5. (a) $Mn_{0.99(2)}Fe_{4.01(2)}Si_3$ neutron powder pattern obtained on POWGEN at 310 K (black) and at 270 K (red) below the ferromagnetic transition. (b) View perpendicularly to the *c*-axis of the $MnFe_4Si_3$

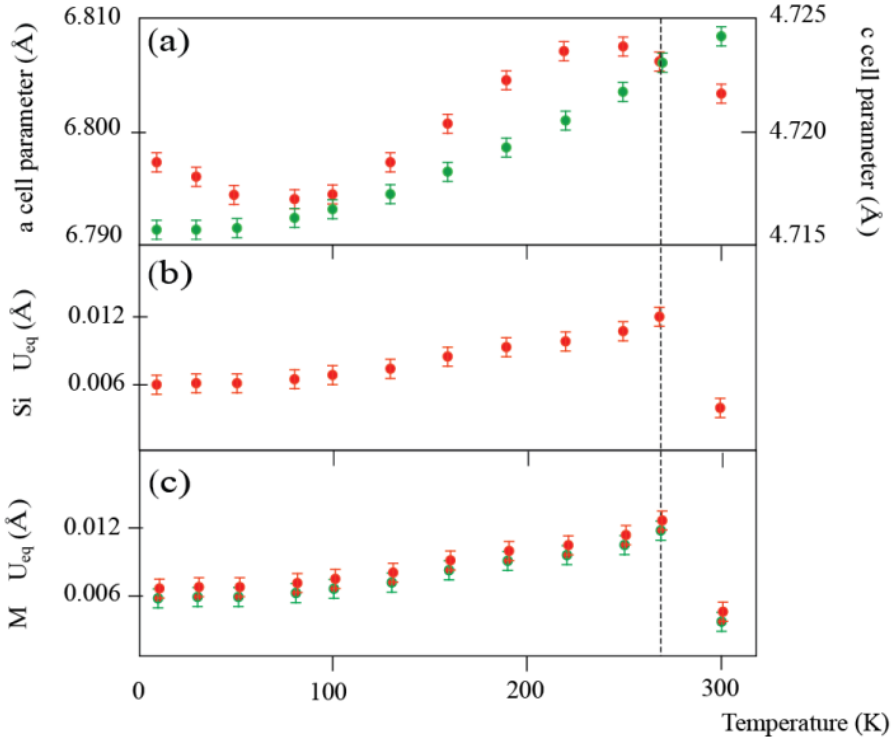

magnetic unit cell refined at 270 K. Red, blue and grey spheres represent M1, M2 and Si atomic sites, respectively. The length of the arrow is scaled to the magnetic moment refined ($0.5\mu_B$ correspond to 1 Å interatomic distance length).

Figure 6. (a) Evolution of the cell parameters (green and red dots represent *c* and (*a*=*b*) cell parameters, respectively), (b) Si ADPs and (c) M ADPs (M1 in green and M2 in red) *vs*. temperature for $MnFe_4Si_3$.

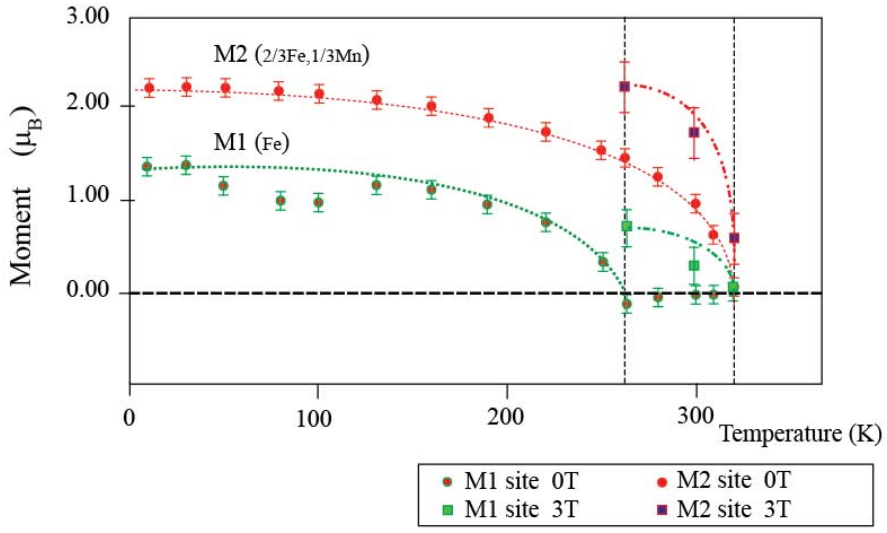

Figure 7. Temperature dependence of the magnetic moments for M1 (green) and M2 (red) sites. Circle and square dots show results refined under no magnetic field and 3 T magnetic field, respectively. (see text for additional details).

In Figure 7 is represented the refined magnetic moments obtained at various temperatures on both M1 and M2 metallic sites. M2 site presents a conventional increase of the magnetic moment ordering as the temperature decreases. The magnetic ordered moment on that site increase up to a value of ~$2.1\mu_B$ in relative good agreement with the previous measurements performed by Songlin et al. [10] At 310 K, the paramagnetic stage fully takes place and the M2 site does not appear to have any magnetic moment ordered. For the M1 site, the magnetic behaviour is different. Indeed, even if the main tendency of the magnetic moments is to increase as the temperature decreases at around 100 K there is a deep "waving" of the magnetic values which is still unexplained and could potentially be associated with the magnetoelastic effect previously

discussed. One interesting feature, in relation with the MCE, is the temperature difference between the two magnetic ordering. Indeed, the magnetic ordering on M1 site appears at around 260 K whereas this phenomenon occurs ~50 K above for the M2 site and corresponds perfectly with the beginning of MCE. Notice finally that at lower temperature, the M1 site magnetic moment converge to a lowest value of ~1.3 μ_B in agreement with the previous measurements performed by polarized neutron study on Fe_5Si_3. [10]

C. Neutron diffraction of $MnFe_4Si_3$ under magnetic field

In order to investigate the influence of the magnetic field on the nuclear/ magnetic structure especially in the vicinity of the magnetic transition, neutron diffraction under magnetic field has been performed on the neutron powder diffractometer HB2A at the High Flux Isotope Reactor at Oak Ridge National Laboratory. As previously in the experimental section the sample has been pelletized to avoid preferred orientation of the grain under magnetic field. The initial data collected at 300 K under no magnetic field are consistent with the results obtained from POWGEN data: cell parameters of a=b= 6.8048(3) Å, c=4.7381(4) Å (Figure 8). The results of this experiment collected under magnetic field (3 Tesla) at 260 and 300 K show strong evidence of an increase in the saturation values of the moments. As illustrated in Figures 7 and 8, a magnetic field of 3 T enhanced the ordering and the orientation of the magnetic moments. In figure 7 is pointed out with some arrows the major peak intensity changes. As notice by the small difference curve, the refinements have quit good goodness of fit of R=3.05% and R=3.21%, under 0 T and under 3 T, respectively. As a first response to the magnetic field, the unit cell slightly stretches of ~1% along the c direction keeping a unit cell volume almost constant. As a second and major effect, local magnetic moment strongly ordered along the c direction, especially on the M1 site below the paramagnetic transition. Therefore and based on this observation, we could assume that the magnetic field is able to perturb/control the small magnetic ordering especially on the low magnetic M1 site at higher temperature than 260 K. This M1 site could act as a “key” to develop the MCE in the temperature range from 260 K to 300 K.

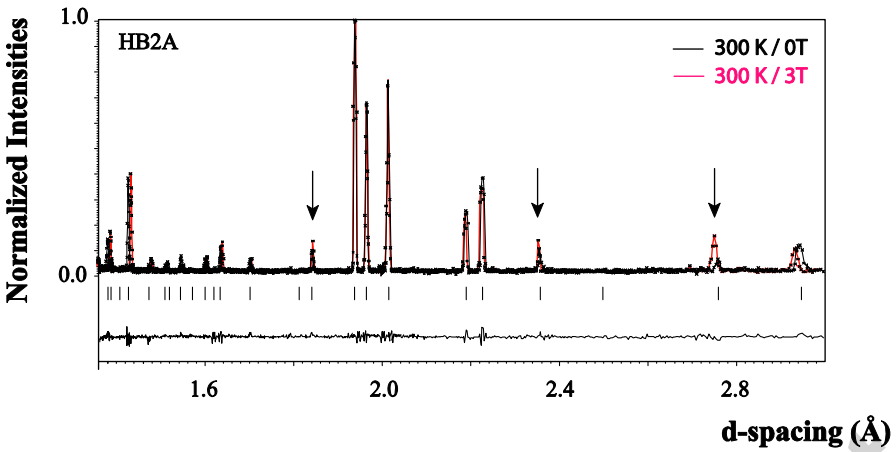

Figure 8. Neutron powder diffraction pattern obtained on HB2A at room temperature under no magnetic field (black curve) and under 3 Tesla (red curve). The arrows indicate the major peak intensities change under magnetic field. (see text for additional details).

We note that at 260 K, the ordered moment per formula unit determined from the refinement of the powder neutron diffraction data at 260 K is 8.0 μ_B (or 1.60μ_B per metal atom) (Figure 7). This is in good agreement with the magnetization measurement shown in Figure 1b. At 270 K and 3 T, a moment of 119 $Am^2.kg^{-1}$ is measured, which is equivalent to 7.7 μ_B per formula unit (or 1.54 μ_B per metal atom).

D. Electronic Structure Calculations.

Theoretical electronic structures of various models of $MnFe_4Si_3$ were determined and analysed to assess the trends in the distribution of Mn and Fe in the structure, which we call the "coloring problem", [33] and to shed some light on the magnetic behaviour of this specific compound. Our preliminary focus was to study the Mn/Fe site distribution into $MnFe_4Si_3$. Band structure calculations on $MnFe_4Si_3$ have been performed on two different models which are necessary approximations to the actual arrangement. Since Fe/Mn the ratio of the M2 site is close to 2/3|1/3, ordering of the Fe and Mn has been created using a symmetrical subgroup of the refined crystallographic space group. The orthorhombic space group P*bcm* has been ideally chosen as subgroup since it allows ordering of Mn and Fe atoms in the 2/3|1/3 ratio. Indeed, using that space group the M1 and M2 positions are equivalently represented by two ($M1_1$ and $M1_2$) and three ($M2_1$, $M2_2$ and $M2_3$) independent crystallographic positions, respectively. The two studied

$MnFe_4Si_3$ models are illustrated in Figure 9 and are presented as follow:

1. Model 1 corresponds to ordering Fe on the $M1_1$, $M1_2$, $M2_1$ and $M2_2$ sites and Mn on the $M2_3$
2. Model 2 corresponds to ordering Fe on the $M1_2$, $M2_1$, $M2_2$, and $M2_3$ sites and Mn on the $M1_1$

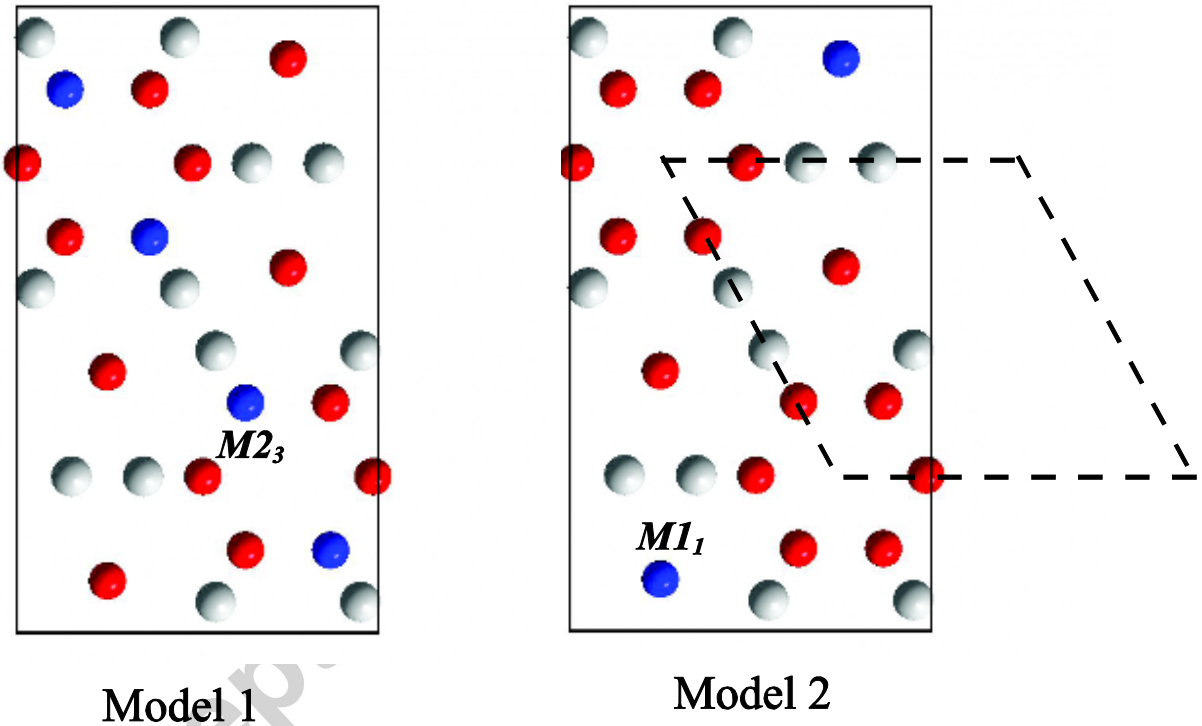

Figure 9.Representation of the $MnFe_4Si_3$ orthorhombic models (Model 1 and Model 2) used for the electronic structure calculations. Red and blue spheres indicate Fe and Mn sites, respectively. In Model 2, the original hexagonal unit cell is illustrated in dash lines.

Nonmagnetic calculation on the $MnFe_4Si_3$ and "Colouring Problem"

Band structures calculations were carried out on these two models under similar conditions (same size of the atomic spheres, same number and size of empty spheres). From the total energies of these two systems, model 1 is 1.4 eV more stable than model 2, which is rather significant even if the value of the total energy, may be contested using the LMTO method. Note that model 1 corresponds to the atomic arrangement refined by neutron powder diffraction.

To understand the relative stability of the model 1 against model 2, total DOS and partial DOS have been calculated for both models. However, both models give a rather similar profile presented on the right side of the Figure 10. The PDOS of the M(Mn/Fe)-3*d* orbitals and Si-4*p* orbitals are represented by green and red thick lines, respectively. The profile of the TDOS is close to the PDOS of the M-3d functions, which suggests that it dominates the electronic properties. The shape of the TDOS in the vicinity of the Fermi level corresponds mostly to two broad peaks: one centered around -2.5 eV and the second one centered on the Fermi level. The Si-4p PDOS is relatively flat with the highest density around -3.5eV, where small bonding interactions occur with the Mn/Fe-3d orbitals. As presented in Figure 4, the M (Mn and Fe) transition metals occupied two different crystallographic sites which are based on octahedral and/ or distorted octahedral sites. Therefore, the two broad peaks previously discussed reflect the (t_{2g}/e_g) orbital splitting which is closer to an (a_1/e'/e") orbital degeneracy due to the distortion toward a trigonal prismatic local environment.

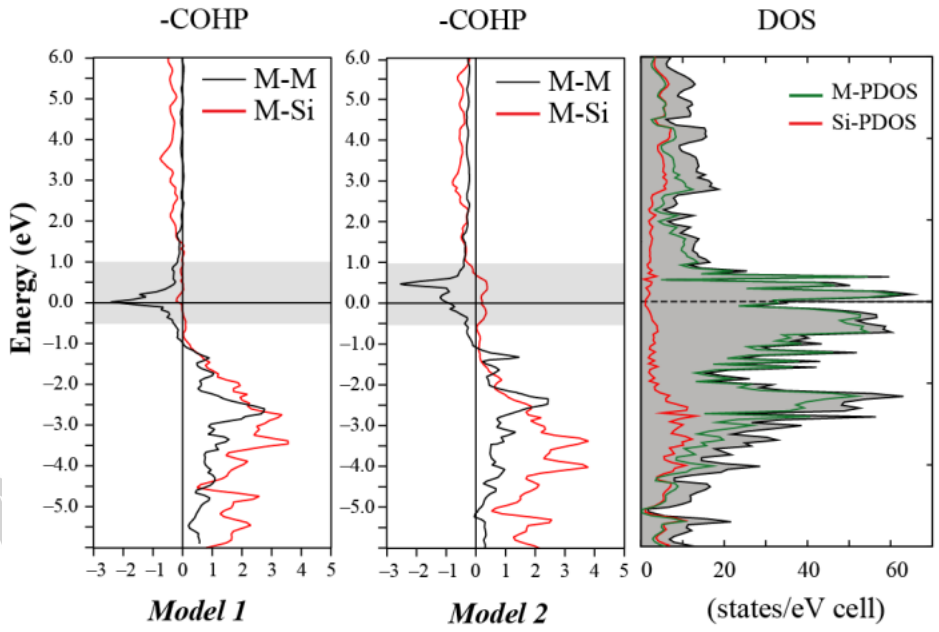

Figure 10. M-Si and M-M COHP curves for the model 1 and model 2 as well as Total DOS and Partial M-DOS and Partial Si-DOS for $MnFe_4Si_3$.

To help understand the relative stability of the Model 1 *vs.* Model 2 the addition of COHP

(crystal overlap Hamilton population [26]) studies have been performed. These COHP curves as presented in Figure 10 are quite useful to analyse the electronic structure, and especially to get insight about the bonding characteristics. In Figure 10 is presented COHP curves of the M-Si and M-M interactions for both models. Using this analysis, it is possible to attribute the first broad peak around -3.5 eV to M-M bonding interactions with a minor Si contribution, whereas the second peak close to the Fermi level corresponds to M-M antibonding states slightly interacting with Si-*p* orbitals. Based on the M-M interactions alone, it is difficult to justify the relative stability of the Model 1 vs. Model 2; however, the M-Si interactions provide additional information. Indeed, Model 1 contrasts with Model 2 by showing some non-bonding M-Si states as compared to antibonding M-Si states at the Fermi level. Therefore, we could assume that the relative stability of Model 1 vs. Model 2 is strongly influenced by the M-Si interactions which are optimized (cross-over between the bonding and antibonding M-Si states) in the preferred model (Model 1).

COHP studies can also be a powerful tool to predict the nature of magnetic interactions in an intermetallic compound such as $MnFe_4Si_3$. Dronskowski et al. have already shown that a driving force for antiferromagnetism or ferromagnetism lies in the local nonbonding or antibonding character of the states around the Fermi level.[34] Such approach has also been used to predict the antiferromagnetism in Mn_5Si_3. [35] In $MnFe_4Si_3$, and as illustrated in Figure 7, the highest populated states correspond to M-M antibonding states. According to the Stoner criteria [36] and on the basis of our previous work,[35,37,38] ferromagnetic properties are expected for $MnFe_4Si_3$, and spin-polarized calculations should be performed to fully understand the electronic structures of such materials. Stoner presented in 1938 a predictive model of itinerant electron ferromagnetism by assuming an average spin field interacting with a single spin. The Stoner criterion can be expressed as follow by:

$$I \times \mathrm{DOS}\,(E_F) > 1$$

where I is a measure of the strength of the exchange interaction in the metal and DOS (E_F) is the density of states at the Fermi level, E_F. Most solid-state physicists still consider the Stoner criterion as a good indicator of whether a metal or an alloy will be ferromagnetic. The DOS(E_F) value is directly accessible by band structure calculations (in our case the DOS(E_F) calculated is

31 states/eV/cell for $MnFe_4Si_3$), and *I* values may be found in various papers. In 1977, Janak was the first one to tabulate the values and his report gives *I* values for various single metals such as Cr (bcc), Mn (fcc), and Fe (bcc) as 0.38, 0.41, and 0.46 eV, respectively. [39] Based on these values, the Stoner criterion for $MnFe_4Si_3$ is approximately 1.25 per Metal atom. This value for the Stoner criterion is only a first approximation because *I* values for each atom are dependent upon the local environment nevertheless it confirms the existence of a spin ordering into the $MnFe_4Si_3$ compound.

Spin-polarized calculations on $MnFe_4Si_3$

To validate our spin-polarized calculations, different initial magnetic models were attempted. However, just one magnetic (ferromagnetic) model was found more stable than the non-magnetic one with a favourable ΔE_{Tot} of 759 meV/unit cell. The atomic magnetic moments obtained from the spin-polarized calculations are listed in table 2. Notice that these values are in good agreement with the ones obtained by the neutron diffraction refined and presented in figure 7.

Table 2. Results of Spin-Polarized Band Structure Calculations obtained for $MnFe_4Si_3$.

M atoms	Magnetic Moment (in μ_B)
Fe1	1.46(2)
Mn2	2.35(2)
Fe2	1.70(2)
Si1	- 0.120(5)
Si2	- 0.115(5)
Si3	-0.007(3)

Total Average magnetic moment of 1.67(2) μ_B per metal atom.

The spin polarized calculations presented in table 2 include a strong negative magnetic polarization on the Si atoms. These magnetic polarizations have already been observed in similar compounds such as Mn_5Si_3 and are usually the sign of some strong hybridization/interaction between the Si(3p)- Mn(3d) orbitals. As compared to the nonmagnetic case (non-polarized), the Si(3p)- Mn(3d) hybridizations increase for the spin-up and decrease for the spin down, due to an

exchange splitting of the *d* block. As a consequence, the number of Si(p) states in the d block above the Fermi level is higher for the spin up that for the spin down and a negative magnetization appears. This observation confirms also the importance of the nature of the non-metal element. To perform a more detail analysis of the electronic/ magnetic interactions associated with the physical properties of $MnFe_4Si_3$, energy band dispersion as well as the TDOS for the majority and minority spin electrons have been calculated and are illustrated in Figure 11. Figure 11 (a) corresponds to the minority (spin-down) direction indicated by ↓ and Figure 11 (b) illustrates the majority (spin-up) direction by ↑. For the minority spin direction ↓, a fatband representation has been used to highlight the contribution of the different d-type orbitals for the M1 and M2 atomic sites. In figure 10(c) is schematically represented the first Brillouin zone with the high symmetry points associated with the hexagonal crystal symmetry of the $MnFe_4Si_3$.

Figure 11 (a) clearly illustrates that most of the ↓ states, especially the ones associated with the d-type orbitals, are occupied. The energy band analysis is primarily showing a strong dispersion along the [ΓA] direction or *c** direction opening a gap of almost 3eV at the A point. The analysis of the bands at this A point indicates that the stabilization at E_F is associated with bonding interactions between the Mn2-d_{xz}, Fe2-d_{xy}/ d_{z2} and Si1-p / Si2-p orbitals whereas the destabilization, at ~ 3eV above E_F, is associated with antibonding interactions mainly from Mn2-d_z^2 and Si1-p_z orbitals. This observation strengthens the previous remarks that the non-metallic element (Si) plays an important part into the electronic/magnetic interactions. It also informs us that even if Mn is the minority metallic element into the compound, its orbitals play a crucial role at the Fermi level contributing strongly to the physical properties of the all materials. The study of the [ΓK],[KM] and [MΓ] directions is also quite interesting since it presents significant Mn2-d_{xy}, Fe1-d_{xy} and Fe2-d_{xy} interactions in the (*a*,b**) reciprocal plane. Based on our crystallographic studies under magnetic field, which suggests a small compression of the unit cell in these directions, it could potentially suggest that these interactions will be emphasized up to opening a small gap. If such assumption is confirmed it will potentially suggest for $MnFe_4Si_3$ a close relation with a half-metallic ferromagnetic behaviour.

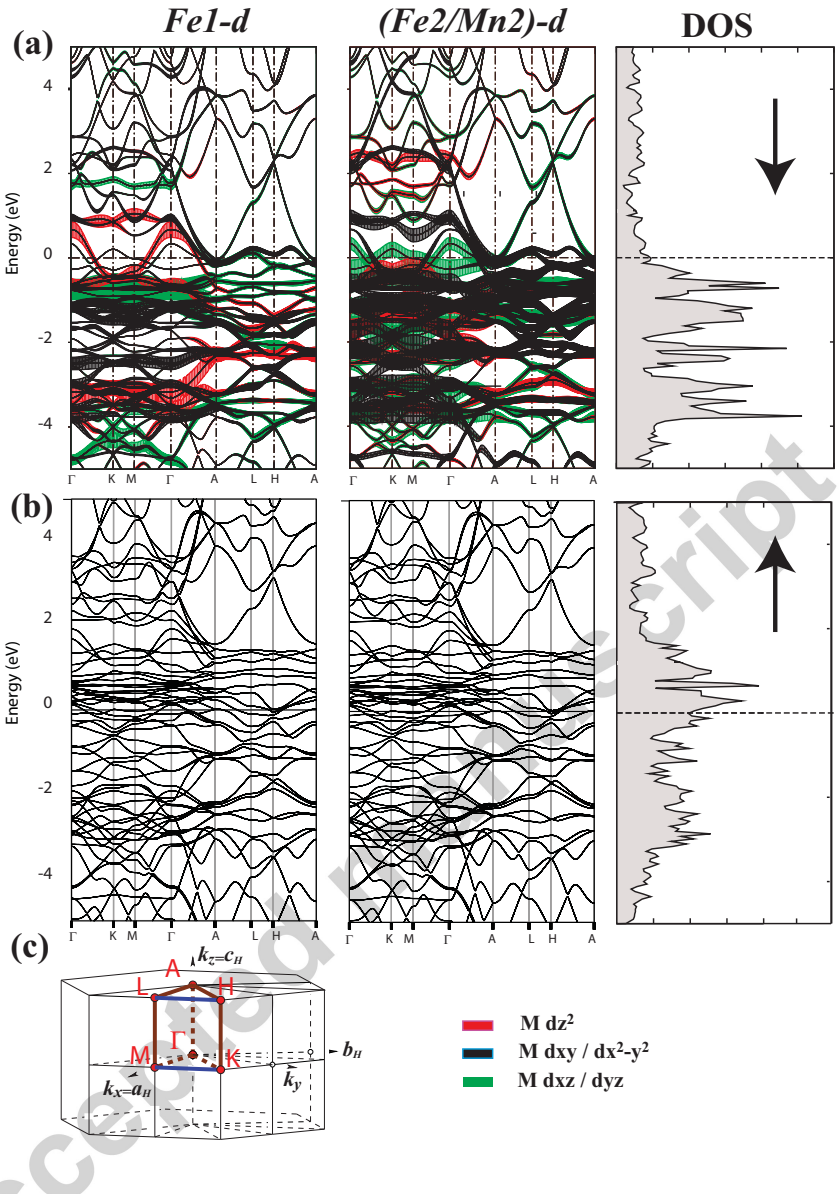

Figure 11. Energy band dispersion of $MnFe_4Si_3$ with some fatband contributions of the various d-type orbitals for the M1 and M2 atomic sites and Total Density of States (TDOS) for the ferromagnetic spin-polarized calculations. See text for additional details.

Half-metallic materials act as a conductor to electrons of one spin orientation, but have a gap at the Fermi level for those of the opposite spin. Although all half-m etals are ferromagnetic, most ferromagnets are not half-metals. Some notable half-metals are CrO_2, Magnetite, Heusler compounds, lanthanum manganite such as La(Ca, Sr, Ba)MnO_3 ,[40] as well as chromium arsenide. Half-metals have attracted some interest for their potential use in spintronics. Among the

compounds previously listed, most of them are also recognized to be the best candidates as magnetocaloric effect materials. [41] If such close relation between half-metallicity and MCE materials is confirmed it could be potentially be a breakthrough in the investigation of new compounds in these two important classes of materials.

Conclusions

The low temperature ferromagnetic ordering in $MnFe_4Si_3$ has been reinvestigated using high resolution neutron powder diffraction and highlights a two-step spin ordering process that we can attribute to the MCE which rises between 280 K and 300 K. Non-spin polarized as well as spin polarized band structure calculations have been used to confirm the site attribution between Mn and Fe but also to validate the ferromagnetic ordering into $MnFe_4Si_3$. Our calculations have also highlighted a possible close relation between MCE and half-metallicity. Further neutron elastic and inelastic experiments are underway to fully elucidate the effect of the magnetic field in this class of materials especially in the light to respond to the question: Is there a relation between half-metallic ferromagnetism and a strong magnetocaloric effect?

Acknowledgements

The authors are grateful to Dr. Jason Hodges and Luke Heroux for their various constructive comments on the neutron experiments measurements. This Research at Oak Ridge National Laboratory's High Flux Isotope Reactor and Spallation Neutron Source was sponsored by the Scientific User Facilities Division, Office of Basic Energy Sciences, U. S. Department of Energy. M.A.M acknowledges support from U.S. Department of Energy, Energy Efficiency and Renewable Energy, Office of Vehicle Technologies, Propulsion Materials Program. Development of the program Jana2006 was supported Praemium Academiae of Czech Academy of Sciences.

References

1. V. K. Pecharsky and K. A. Jr Gschneidner, *Adv. Mater.*, 2001, **13**, 683.
2. V. K. Pecharsky and K. A. Jr Gschneidner, *Phys. Rev. Lett.,* 1997, **78**, 4494.
3. V. K. Pecharsky and K. A. Jr Gschneidner, *J. Magn. Magn. Mater.*, 1997 **167**, L179.
4. V. K. Pecharsky and K. A. Jr Gschneidner, *Appl. Phys. Lett*., 1997 **70**, 3299.
5. W. Choe, G. J. Miller, J. Meyers, S. Chumbley, and A. O. Pecharsky, *Chem. Mater*., 2003 **15**, 1413.
6. E.Brück, O. Tegus, D. T. Cam Thanh, Trung, T. Nguyen, K. H. J. Buschow, *Inter. J. of Refrigeration*, 2008, 763.
7. E. Brück, M. Ilyin, O. Tegus, *J. Mag. Magn. Mat.,* 2005, **290**, 8.
8. K. A. Jr. Gschneidner, V. K. Pecharsky, O. A. Tsokol, *Reports on the Progress in Physics* 2005, **68**, 1479.
9. S. Lin, O. Tegus, E. Brück, W. Dagula, T. J. Gortenmulder, K. H. J. Buschow, *IEEE Transactions on Magnetics*, 2006, **42**(13), 3776.
10. Songlin, W.Dagula, O. Tegus, E. Brück, J. C. P. Klaasse, F. R. de Boer and K. H. J.Buschow, *J. Alloys Compd*., 2002, **334**(1-2), 249.
11. Ronald J.Sovie and George R. Seikel, Radio-frequency induction heating of low-pressure plasmas. Washington, D.C.: National Aeronautics and Space Administration; Springfield, Va.: Clearinghouse for Federal Scientific and Technical Information, October 1967.
12. A. Huq, J. P. Hodges, O. Gourdon and L. Heroux, *Z. Kristallogr. Proc. 1*, 2011, 127.
13. V. O. Garlea, B. C. Chakoumakos, S. A. Moore, G. B. Taylor, T. Chae, R. G. Maples, R. Riedel, G. W. Lynn and D. Selby, "Overview of the High-Resolution Powder Diffractometer at the High Flux Isotope Reactor," *Applied Physics A*, 2010, **99**, 531.
14. V. Petricek, M. Dusek and L. Palatinus, Jana2006; The crystallographic computing system. Institute of Physics, Praha, Czech Republic, 2006.
15. H. Binczycka, Z. Dimitrijevic, B. Gajic, A. Szytula *Phys. Status Solidi A* 1973 **19**, K13.
16. V. Petricek, J. Fuksa, and M. Dusek, *Acta Cryst.* 2010 **A66**, 649.
17. J-M. Perez-Mato, J. L. Ribeiro, V. Petricek and M I. Aroyo, *J Phys. Condens. Matter* 2012, **24**, 163201.

18. O. K. Andersen, O. Jepsen, *Phys. Rev. Lett.* 1984, **53**, 2571.
19. O. K. Andersen, *Phys. Rev*. 1975, **B12**, 3060.
20. O. K. Andersen, O. Jepsen, D. Glötzel, In Highlights of Condensed-Matter Theory; F. Bassani, F. Fumi, M. P. Tosi, W. R. L. Lambrecht, Eds.; North-Holland: New York, 1985.
21. O. K. Andersen, *Phys. Rev.* 1986, **B34**, 2439.
22. The Stuttgart Tight-Binding LMTO-ASA program, version 4.7; Max-Planck-Institut für Festkrperförschung: Stuttgart, Germany, 1998.
23. U. Von Barth and L. J. Hedin, *Phys. C* 1972, **5**, 1629.
24. D. D. Koelling and B. N. J. Harmon, *Phys. C* 1977, **10**, 3107.
25. O. Jepsen, O. K. Anderson, *Z. Phys. B* 1995, **97**, 35.
26. R. Dronskowski, and P. E. Blöchl, *J. Phys. Chem*. 1993, **97**, 8617.
27. P. E. Blöchl, O. Jepsen, O. K. Andersen, *Phys. Rev.* 1994, **B49**, 16223.
28. R. D. Mc Michael, J. J. Ritter and R. D. Shull *J. Appl. Phys.* 1993, **73**, 6946.
29. S. Yu Dan'kov, T. I. Ivanova, and A. M. Tishin, *J. Magn. Magn. Mater.* 1996, **152**, 208.
30. V. K. Pecharsky and K. A. Jr Gschneidner *J. Appl. Phys.,* 1999, **86**, 565.
31. J. Yao and Y. Mozharivskyj, *Z. Anorg. Allg. Chem*. 2011, **637**(13), 2039.
32. M. Herlitschke, M. Gottschlich, B. Klobes, J. Voigt, J. Perßon, H.-C. Wille, K. Schlage, T. Brückel and R. Hermann 2012, unpublished work.
33. G. J. Miller, *Eur. J. Inorg. Chem*.,1998, **5**, 523.
34. G. A. Landrum and R. Dronskowski, *Angew. Chem*., Int. Ed. 2000, 1560.
35. M. Gottschlich, O. Gourdon, J. Perßon, C. de la Cruz, V. Petricek and T. Brückel, *J. Mater. Chem*. 2012, **22**, 15275.
36. E. C. Stoner, *Proc. R. Soc. London* 1938, **165**, 372.
37. O. Gourdon and G. J. Miller, *J. Solid State Chem*. 2003, **173**, 137.
38. O.Gourdon, S. Bud'ko, D. Williams and G. J. Miller, *Inorg. Chem.* 2004, **43**, 3210.
39. J. F. Janak *Phys. Rev. B* 1977, **16** (1), 255.
40. J. M. D. Coey and M. Venkatesan, *J. Appl. Phys*. 2002, **91** (10): 8345
41. A. M. Tishin and Y. I. Spichkin "The Magnetocaloric effect and its applications" 2003 Institute of Physics publishing- Series in Condensed Matter Physics.

Table Of Contents

Theoretical and experimental reinvestigation of the magnetic structure of $MnFe_4Si_3$ for a better understanding of its large magnetocaloric effect (MCE).

- Strong magnetic transition from paramagnetism to ferromagnetism at about 302(2) K.
- MCE associated to a partial reordering of the spins between ~270 K and 300 K.
- DFT calculations show strong relation between MCE and spintronic materials.

Keywords: Magnetocaloric effect Materials, Intermetallic, Silicide, Magnetism, Neutron Diffraction, Density Functional Theory